

Displacement damage of the space broad-spectrum proton in semiconductor materials

Yue-Qian Jiang(姜月千), Li-Chao Tian(田立朝), Guo-Bo Zhang(张国博), Run-Zhou Yu(余润洲), Bi-Hao Xu(徐碧浩), Xiang-Cheng Li(李翔城), Yan-Qing Deng(邓彦卿), De-Bin Zou(邹德滨), Tong Wu(吴桐), Yan-Yun Ma(马燕云), and Xiao-Hu Yang(杨晓虎)

Citation: Chin. Phys. B, 2025, 34 (**10**): 106103. DOI: 10.1088/1674-1056/adf9fb
http://cpb.iphy.ac.cn; http://iopscience.iop.org/cpb

What follows is a list of articles you may be interested in

Molecular dynamics simulations of collision cascades in polycrystalline tungsten

Lixia Liu(刘丽霞), Mingxuan Jiang(蒋明璇), Ning Gao(高宁), Yangchun Chen(陈阳春), Wangyu Hu(胡望宇), and Hiuqiu Deng(邓辉球)

Chin. Phys. B, 2025, 34 (**4**): 046103. DOI: 10.1088/1674-1056/adb410

Sensitivity investigation of 100-MeV proton irradiation to SiGe HBT single event effect

Ya-Hui Feng(冯亚辉), Hong-Xia Guo(郭红霞), Yi-Wei Liu(刘益维), Xiao-Ping Ouyang(欧阳晓平), Jin-Xin Zhang(张晋新), Wu-Ying Ma(马武英), Feng-Qi Zhang(张凤祁), Ru-Xue Bai(白如雪), Xiao-Hua Ma(马晓华), and Yue Hao(郝跃)

Chin. Phys. B, 2024, 33 (**1**): 016104. DOI: 10.1088/1674-1056/acf303

Neutron-induced single event upset simulation in Geant4 for three-dimensional die-stacked SRAM

Li-Hua Mo(莫莉华), Bing Ye(叶兵), Jie Liu(刘杰), Jie Luo(罗捷), You-Mei Sun(孙友梅), Chang Cai(蔡畅), Dong-Qing Li(李东青), Pei-Xiong Zhao(赵培雄), and Ze He(贺泽)

Chin. Phys. B, 2021, 30 (**3**): 036103. DOI: 10.1088/1674-1056/abccb3

Geant4 simulation of proton-induced single event upset in three-dimensional die-stacked SRAM device

Bing Ye(叶兵), Li-Hua Mo(莫莉华), Tao Liu(刘涛), Jie Luo(罗捷), Dong-Qing Li(李东青), Pei-Xiong Zhao(赵培雄), Chang Cai(蔡畅), Ze He(贺泽), You-Mei Sun(孙友梅), Ming-Dong Hou(侯明东), Jie Liu(刘杰)

Chin. Phys. B, 2020, 29 (**2**): 026101. DOI: 10.1088/1674-1056/ab5fc4

Investigation of flux dependent sensitivity on single event effect in memory devices

Jie Luo(罗捷), Tie-shan Wang(王铁山), Dong-qing Li(李东青), Tian-qi Liu(刘天奇), Ming-dong Hou(侯明东), You-mei Sun(孙友梅), Jing-lai Duan(段敬来), Hui-jun Yao(姚会军), Kai Xi(习凯), Bing Ye(叶兵), Jie Liu(刘杰)

Chin. Phys. B, 2018, 27 (**7**): 076101. DOI: 10.1088/1674-1056/27/7/076101

Displacement damage of the space broad-spectrum proton in semiconductor materials

Yue-Qian Jiang(姜月千)[1,†], Li-Chao Tian(田立朝)[1,†], Guo-Bo Zhang(张国博)[1,‡], Run-Zhou Yu(余润洲)[1], Bi-Hao Xu(徐碧浩)[1], Xiang-Cheng Li(李翔城)[2], Yan-Qing Deng(邓彦卿)[2], De-Bin Zou(邹德滨)[1], Tong Wu(吴桐)[2], Yan-Yun Ma(马燕云)[3,4], and Xiao-Hu Yang(杨晓虎)[1,§]

[1] *College of Science, National University of Defense Technology, Changsha* 410073, *China*
[2] *College of Advanced Interdisciplinary Studies, National University of Defense Technology, Changsha* 410073, *China*
[3] *School of Automation and Electronic Information, Xiangtan University, Hunan* 411105, *China*
[4] *School of Physics and Electronics, Hunan University, Changsha* 410082, *China*

(Received 10 June 2025; revised manuscript received 30 July 2025; accepted manuscript online 11 August 2025)

Displacement damage induced by high-energy protons in the space radiation environment presents a serious risk to the reliability of spacecraft materials and onboard electronics. Nevertheless, studies on displacement damage induced by space-based broad-spectrum protons are still limited. In this paper, the nonionizing energy loss (NIEL) of space broad-spectrum protons at different orbital altitudes in semiconductor materials is investigated using Geant4 Monte Carlo simulations. We find that the NIEL of silicon (Si) and gallium arsenide (GaAs) first increases and then decreases with orbital altitude, and that shielding effects can result in either the saturation or continuous increase of NIEL, depending on the shielding layer thickness. A fast NIEL calculation method for arbitrary broad spectra is proposed based on statistical probability principles and the effective proton proportion. Meanwhile, a more uniform spatial distribution of mean damage energy per source particle ($T_{\rm dam}$) deposition from broad-spectrum protons can be achieved by increasing the shielding layer thickness and lowering the orbital altitude. Notably, the relative contribution of displacement damage caused by nuclear reactions decreases with increasing orbital altitude and shielding layer thickness. The results provide a quantitative reference for space displacement damage in semiconductor materials.

Keywords: nonionizing energy loss, space broad-spectrum protons, shielding layer, Geant4

PACS: 61.80.–x, 61.80.Jh, 61.82.Fk, 42.88.+h

DOI: 10.1088/1674-1056/adf9fb **CSTR:** 32038.14.CPB.adf9fb

1. Introduction

High-energy protons constitute a significant component of solar cosmic rays, galactic cosmic rays, and Earth's outer radiation belts. Upon penetrating spacecraft shielding, these protons interact with onboard electronic systems through both ionizing and non-ionizing energy loss mechanisms.[1–3] The resulting energy deposition generates structural defects in semiconductor lattices,[3–7] which leads to progressive degradation of electrical characteristics, ultimately compromising spacecraft reliability and operational lifespan.[1,2,8–16] This fundamental radiation damage phenomenon is formally classified as displacement damage. The investigation of proton-induced displacement damage in semiconductor materials is a critical research focus for spacecraft durability and operational reliability assessment. Many works have demonstrated that the accumulation of radiation-induced defects through displacement damage serves as the primary driver of parametric degradation in electronic components.[1,2,17–20] Different particle species (electrons, protons, neutrons, and gamma rays) show fundamentally distinct interaction mechanisms with matter, resulting in divergent energy deposition distributions and varying degrees of radiation-induced damage. To enable quantitative comparison of displacement damage across different particle species and fluences, researchers have adopted a standardized defect density metric known as the displacement damage dose (DDD). It is formally defined as the product of the non-ionizing energy loss (NIEL) and the particle fluence φ (that is, DDD $= \varphi \times$ NIEL), where NIEL represents the energy deposited per unit mass thickness (MeV·cm^2·g^{-1}) through atomic displacement processes.[17,21–26] A large number of experiments have demonstrated that a linear relationship exists between defect density and DDD in Si-based devices, thereby establishing DDD as a universal standard for displacement damage assessment.[1,14,27–29] Through the NIEL-fluence equivalence principle, radiation damage induced by different particle species and energies can be systematically normalized to equivalent DDD values, significantly improving the accuracy of cross-environment damage prediction models.

At present, studies on displacement damage mainly focus on monoenergetic proton irradiation as well as

†These authors contributed equally to this work.
‡Corresponding author. E-mail: zgb830@163.com
§Corresponding author. E-mail: xiaohu.yang@aliyun.com

© 2025 Chinese Physical Society and IOP Publishing Ltd. All rights, including for text and data mining, AI training, and similar technologies, are reserved.

its mechanisms and impact on radiation-induced material degradation.[3,16,30–35] Meanwhile, molecular dynamics simulations and experimental approaches have been employed to investigate displacement threshold energy dependencies and defect evolution kinetics. However, studies on displacement damage induced by broad-spectrum protons remain limited, as monoenergetic protons cannot account for the multi-energy composition.[36–39] In practical radiation environments, both natural and artificial, proton energy spectra show significant complexity and diversity, which is different from proton energy spectra generated by ground-based radiation damage testing facilities including nuclear reactors, traditional particle accelerators, and laser-driven particle accelerators.[40–45] This mismatch between idealized experiments and practical radiation environments identifies a crucial knowledge gap in displacement damage understanding.

In this paper, the displacement damage induced by broad-spectrum protons in silicon (Si) and gallium arsenide (GaAs) materials under varying shielding layer thicknesses and orbital altitudes is investigated. The effective proton proportion of the broad spectrum is defined, and a fast calculation method is proposed to evaluate the NIEL in semiconductor materials. Furthermore, we investigate the effect of the shielding layer on the deposition of $T_{\rm dam}$, and the relative contributions of elastic and inelastic collisions to NIEL at different orbital altitudes.

2. Theoretical method and verification

2.1. Calculation method of NIEL

The NIEL quantifies the energy transferred from incident particles to target nuclei via Coulomb and nuclear elastic or inelastic collisions, and is directly proportional to displacement damage. This means that higher NIEL values correspond to an increased defect generation rate due to enhanced atomic displacement cascades. This relationship can be expressed as[25]

$$\mathrm{NIEL}(E) = \frac{N_{\rm A}}{M_2}\int_{E_{\rm d}}^{E_{\rm max}} E\,(\mathrm{d}\sigma/\mathrm{d}E)\,f_{\rm n}(E)\,\mathrm{d}E. \tag{1}$$

where E is the incident particle energy, $N_{\rm A} = 6.022\times10^{23}$ is Avogadro's constant, M_2 is the atomic mass of the target material, $E_{\rm d}$ is the threshold energy of the Frenkel pair (FP) generated in the material, $\mathrm{d}\sigma/\mathrm{d}E$ is the differential cross section for a recoil atom with energy E, $E_{\rm max}$ is the maximum energy transferred from the incident particle to the recoil atom, and $f_{\rm n}$ is the damage partition factor. When accounting for atomic recoil, the NIEL formula can be modified as[36]

$$\mathrm{NIEL}(E) = \frac{N_{\rm A}}{A}\sum_i \sigma_i(E)\,E_{\rm dam}(E), \tag{2}$$

where A is the mass number of the target atom, $\sigma_i(E)$ is the reaction cross section of the i-th recoiling atom, and $E_{\rm dam}(E) = E\times f_{\rm n}(E)$ is the non-ionizing damage energy transferred by a recoil atom with energy E in the material. To further refine the calculation, Jun *et al.*[36] introduced the mean damage energy per source particle, defined as $T_{\rm dam} = N_{\rm v}h\sum_i \sigma_i(E)E_{\rm dam}(E)$, where $N_{\rm v}$ is the atomic number density and h is the thickness of the target material. Thus, the NIEL can be expressed as[36]

$$\mathrm{NIEL}(E) = T_{\rm dam}/(\rho h). \tag{3}$$

For a broad energy spectrum of incident protons, the NIEL can be calculated by integrating over the energy distribution[46]

$$\mathrm{NIEL}_{\rm spectrum} = \frac{\int_{E_{\rm min}}^{E_{\rm max}} \mathrm{NIEL}(E)\,\varphi(E)\,\mathrm{d}E}{\int_{E_{\rm min}}^{E_{\rm max}} \varphi(E)\,\mathrm{d}E}. \tag{4}$$

2.2. Model construction and verification

In order to study the displacement damage in materials caused by space protons, we calculate the NIEL at different orbital altitudes using the Geant4 code.[47,48] By employing the QGSP_BIC physical model,[5,35,49] the G4IonINCLXXPhysics list,[47,48] and the G4ScreenedNuclearRecoil class,[50] Geant4 can accurately simulate particle transport processes, including electromagnetic and hadronic interactions, nuclear reactions, as well as displacement effects. In our simulations, $E_{\rm d}$ is assigned as 21 eV for Si, 10 eV for Ga, and 10.8 eV for As, consistent with the calculations reported in Jun's work.[23] A planar proton source geometrically matched to the material cross-section is used for irradiation simulations. Within the Geant4 stochastic energy sampling framework, the simulation configuration consisted of 10^9 incident protons and 20 independent Monte Carlo iterations to ensure statistical robustness and comprehensive spectral sampling.

Si and GaAs are selected as target materials due to their widespread use in spacecraft applications. The thicknesses of these materials vary across different devices depending on functional requirements.[51–53] To simplify the model, this study focuses on semiconductor substrates commonly used in spacecraft chips and solar cells, with a standardized thickness of 500 μm and a cross-sectional area of 5 cm × 5 cm to satisfy the thin-target approximation. The effect of varying thicknesses is further investigated in subsequent analyses. To account for different shielding scenarios in spacecraft systems, three configurations are examined: no shielding, 254 μm (10 mil) Al shielding (representing thin structural shielding within devices), and 2.54 mm (100 mil) Al shielding (simulating spacecraft hull protection). Additional shielding thicknesses were evaluated in the development of the fast NIEL calculation method.

To validate the reliability of the NIEL calculation approach, the thin-target approximation method is employed to systematically evaluate the NIEL values for monoenergetic protons in the energy range of 0.1–1000 MeV interacting with Si and GaAs materials. These results are benchmarked against

reference datasets reported by Jun *et al.*,[23] Bai *et al.*,[39] and Summer *et al.*,[54] with the comparative results presented in Fig. 1. Numerical analysis shows strong agreement in the variation of NIEL values with incident proton energy. The quantitative validation confirms the applicability of the model for evaluating proton-induced NIEL in Si and GaAs materials, thereby establishing a reliable reference baseline for subsequent NIEL calculations under various orbital proton spectra in different materials.

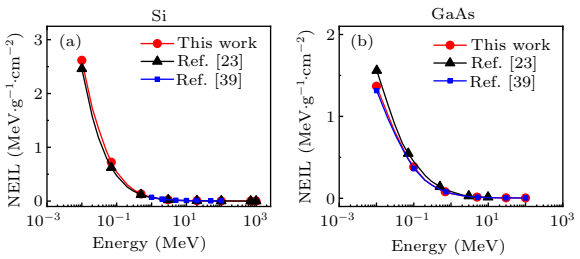


Fig. 1. The NIEL of incident protons as a function of incident proton energy for (a) Si and (b) GaAs.

3. Simulation results and discussion

3.1. The distribution of space proton energy spectra

Figure 2 shows space proton energy spectra at different orbital altitudes calculated using the AP8 model[55] from SPENVIS,[56] representing the accumulated integral fluxes over a one-year period. To simplify orbital dynamics analysis, we employ a circular orbit with equal perigee and apogee radii and an orbital inclination of 0°. One can see that both the maximum and average proton energies decrease with increasing orbital altitude due to geomagnetic-field shielding effects. Meanwhile, the flux of high-energy protons decreases, whereas that of low-energy protons increases. At an orbital altitude of 16000 km, the flux of 200 MeV protons is 10^{-12} times that of 0.5 MeV protons. In addition, the shape of the energy spectrum evolves from a single-temperature distribution to a complex exponential broad spectrum.

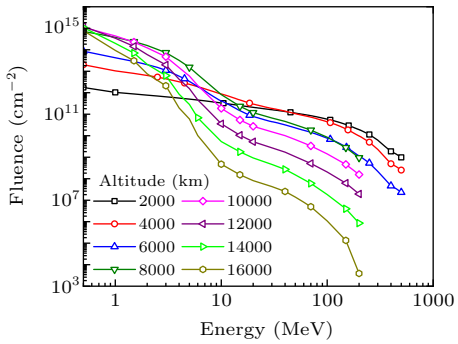


Fig. 2. Space proton energy spectra at different orbital altitudes, calculated using the AP8 model (cumulative 1-year integral fluxes of protons).

3.2. The energy deposition characteristics of monoenergetic protons

We first use the SRIM code[57] to study the stopping power and energy deposition of protons, and then use Geant4 to calculate the NIEL distribution of monoenergetic protons with different energies in Si. Figure 3(a) shows the evolution of electronic and nuclear stopping powers. One can see that both Coulomb elastic scattering cross-sections and nuclear elastic scattering cross-sections exhibit inverse energy dependence, i.e., decreasing with increasing proton energy. This indicates that the energy deposition under both scattering mechanisms exhibits Bragg peak characteristics, as shown in Fig. 3(b). Under monoenergetic proton irradiation conditions, energy deposition is predominantly localized near the end of the proton range. This spatial confinement characteristic is similarly observed in non-ionizing energy deposition, as shown in Fig. 3(c). When the proton range is less than the thickness of the material, the proton energy is completely deposited in the material, which leads to the maximum NIEL. However, when the incident proton range exceeds the material thickness, the deposited energy only constitutes a small fraction of the total proton energy due to the Bragg peak effect, so the non-ionizing energy deposition is significantly decreased compared with the total energy deposition. It should be noted that the distribution of non-ionizing energy deposition becomes more complex under the irradiation condition of space broad energy spectrum protons. Although a large number of low-energy protons predominate in space, their limited kinetic energy restricts the generation of secondary particles in the material. Therefore, the predominant contribution of non-ionizing energy deposition originates from protons with ranges approximating the material thickness, namely, effective protons (EP). To account for the inherent range straggling phenomenon in proton irradiation, the EP are defined as protons with ranges between 10% and 120% of the material thickness. The selection of the minimum and maximum thresholds depends on the higher correlation coefficient in statistical theory (not shown here). Figure 3(d) shows the NIEL

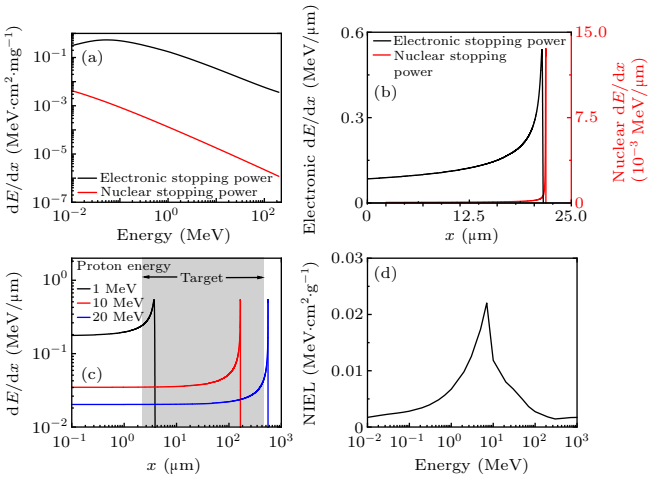


Fig. 3. Stopping power, energy deposition, and NIEL distribution of monoenergetic protons in silicon. (a) Ionization and nuclear stopping powers as functions of proton energy. (b) Energy deposition distribution for 3 MeV protons: ionization and nuclear contributions. (c) Energy deposition distribution and (d) NIEL of protons with various energies in a 500-μm-thick silicon target.

of monoenergetic protons with different energies in a fixed 500-μm-thick target. Notably, the NIEL of EP within the 3–10 MeV range significantly exceeds that of both lower energy protons (< 0.1 MeV) and higher energy protons (> 50 MeV).

4. Displacement damage under varying shielding layer thicknesses and orbital altitudes

4.1. NIEL analysis

A shielding layer can effectively mitigate radiation damage to semiconductor devices from broad-spectrum proton beams in orbit. However, the evolution of NIEL exhibits distinct behaviors at different orbital altitudes under varying shielding thicknesses. Figures 4(a) and 4(b) show the NIEL of broad energy spectrum proton beams in Si (a) and GaAs (b) as a function of orbital altitude, where the black, red, and blue lines represent 2.54 mm aluminum shielding, 254 μm aluminum shielding, and no shielding, respectively. The circles in (a) and (b) represent the theoretical values derived from Eq. (4), and the curves represent the simulation results. One can see that the theoretical values agree well with the simulation results. For the case of no shielding, the NIEL of both materials increases initially and then decreases with increasing orbital altitude, reaching a maximum of 0.01059 MeV·cm^2/g at an orbital altitude of 5000 km for Si and 0.0067 MeV·cm^2/g at 4000 km for GaAs. This results from altitude-dependent variation in the proportion of EP. However, with 254 μm aluminum shielding, the NIEL of both materials increases initially and then approaches saturation. Meanwhile, one can note that adding a relatively thin shielding layer does not effectively reduce NIEL. For the case of 2.54 mm Al shielding, both materials show a monotonic increase in NIEL with orbital altitude. This is because the shielding layer modifies the energy spectrum of protons incident on the material. With increasing shielding thickness, the attenuation of low-energy protons is significantly enhanced, as shown in Figs. 4(c) and 4(d), resulting in a corresponding change in the EP proportion α_p. Figures 4(e) and 4(f) show the evolution of the EP proportion α_p with different orbital altitudes under different shielding thicknesses. One can see that the variation trend of α_p with orbital altitude is consistent with that of NIEL, which demonstrates a strong correlation between EP and NIEL. It is worth noting that the displacement damage from orbital electrons has been excluded from consideration, as proton-induced damage dominates by multiple orders of magnitude.

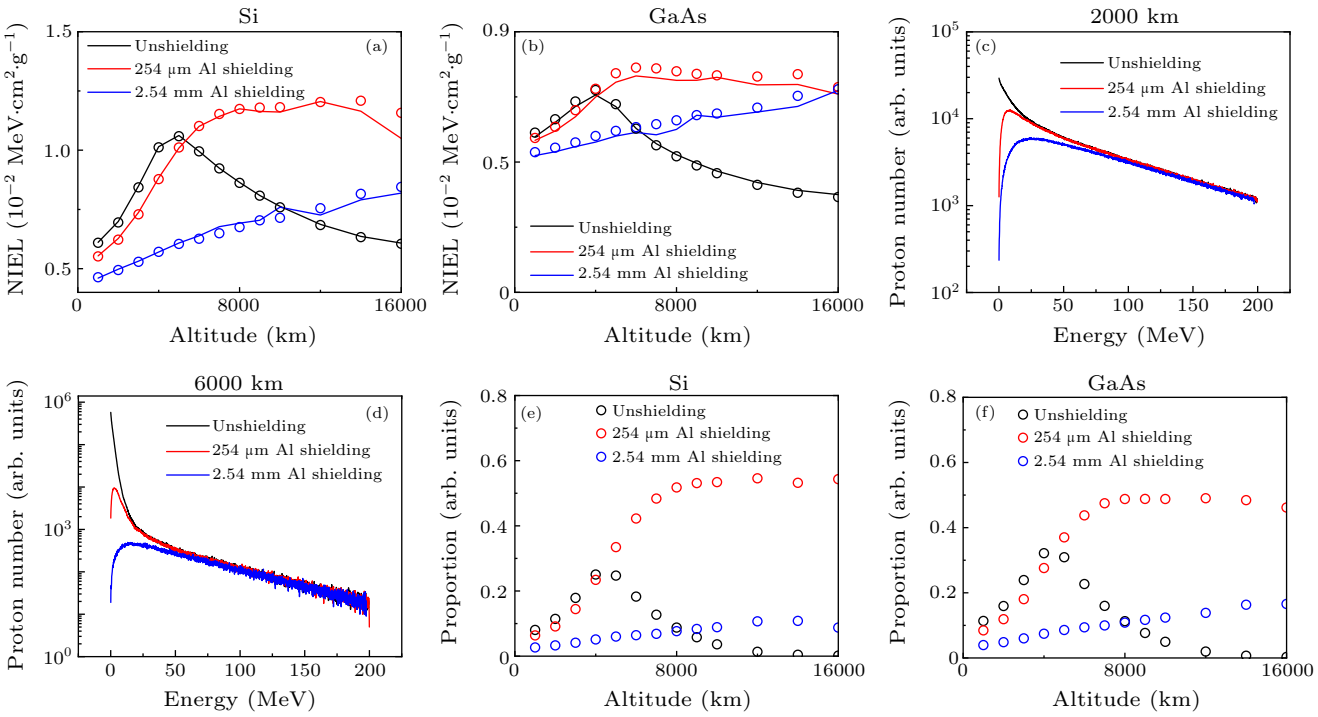


Fig. 4. Evolution of NIEL with different orbital altitudes for various shielding layer thicknesses in a 500 μm-thick (a) Si and (b) GaAs. (c) and (d) Proton energy spectra under varying shielding conditions at orbital altitudes of 2000 km, 6000 km, and 10000 km, respectively. (e) and (f) Evolution of the effective proton proportion α_p with orbital altitude for different shielding layer thicknesses in (e) Si and (f) GaAs.

In order to clarify the quantitative relationship between NIEL and α_p, we also investigate the linear and Gaussian broad-spectrum protons, along with shielding configurations using Al and SiO_2 at thicknesses of 20 μm, 50 μm, 100 μm, and 500 μm (not shown here). The results show trends consistent with the orbital broad-spectrum and are subsequently employed in further analyses. We find a statistically significant linear correlation between the square root of α_p and NIEL in Si, i.e., $S_a = \sqrt{\alpha_p}$, as shown in Fig. 5. The relationship between S_a and NIEL in GaAs is similar.

Taking Si as an example, regression analysis of the data in Fig. 5 yields a Pearson correlation coefficient $R =$

0.96648. The fitted linear regression parameters are intercept $b = 0.00374 \pm 2.14955 \times 10^{-4}$ and slope $k = 0.01079 \pm 4.71329 \times 10^{-4}$. These results demonstrate a statistically significant linear correlation, consistent with the dominant role of S_a in spectral-dependent displacement damage. Therefore, for a given broad energy spectrum, the NIEL can be expressed as

$$\mathrm{NIEL}_{\mathrm{spectrum}} = b + k\sqrt{\alpha_p}. \tag{5}$$

Accordingly, NIEL can be approximated based on α_p. The method is fast and can be applied to the interaction between broad-spectrum protons and materials. For example, once the incident energy spectrum and material thickness are specified, we calculate $\mathrm{NIEL}_{\mathrm{spectrum}}$ using Eq. (5) and subsequently determine the DDD through $\mathrm{DDD} = \varphi \times \mathrm{NIEL}_{\mathrm{spectrum}}$. This DDD is then applied to characterize the radiation-induced degradation in triple-junction solar cells, where the normalized maximum power degradation follows the relation $P_{\max}/P_{\max 0} = 1 - C \cdot \log(1 + D/D_0)$.[51]

The target material thickness is inherently accounted for in the EP proportion calculation, resulting in distinct intercepts and slopes for different thicknesses, as shown in Fig. 6. Figure 6 demonstrates two key thickness-dependent effects: an expansion of the 95% prediction band area, and a reduction in the slope of the fitted curve. These trends originate from the broadening EP distribution with increasing thickness. As the EP range widens, a greater proportion of particles with lower NIEL values contribute to α_p, consequently reducing the relative impact of high-NIEL protons. This fundamental mechanism simultaneously explains both the prediction band broadening and slope attenuation phenomena.

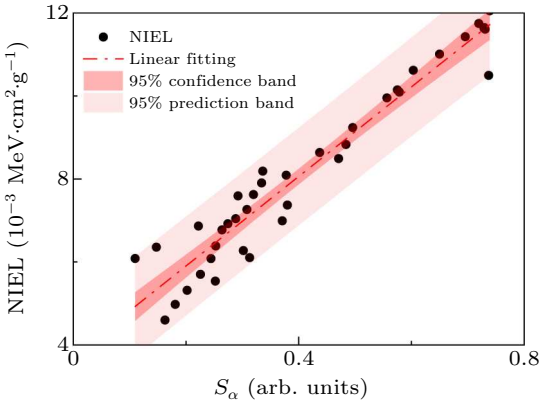


Fig. 5. Correlation between NIEL in Si and S_α. Black solid circles represent simulation results. The red region with 50% transparency indicates the 95% confidence band of the fitted curve. The red region with 70% transparency shows the 95% prediction band for new data points. The dash-dotted line indicates the linear fit.

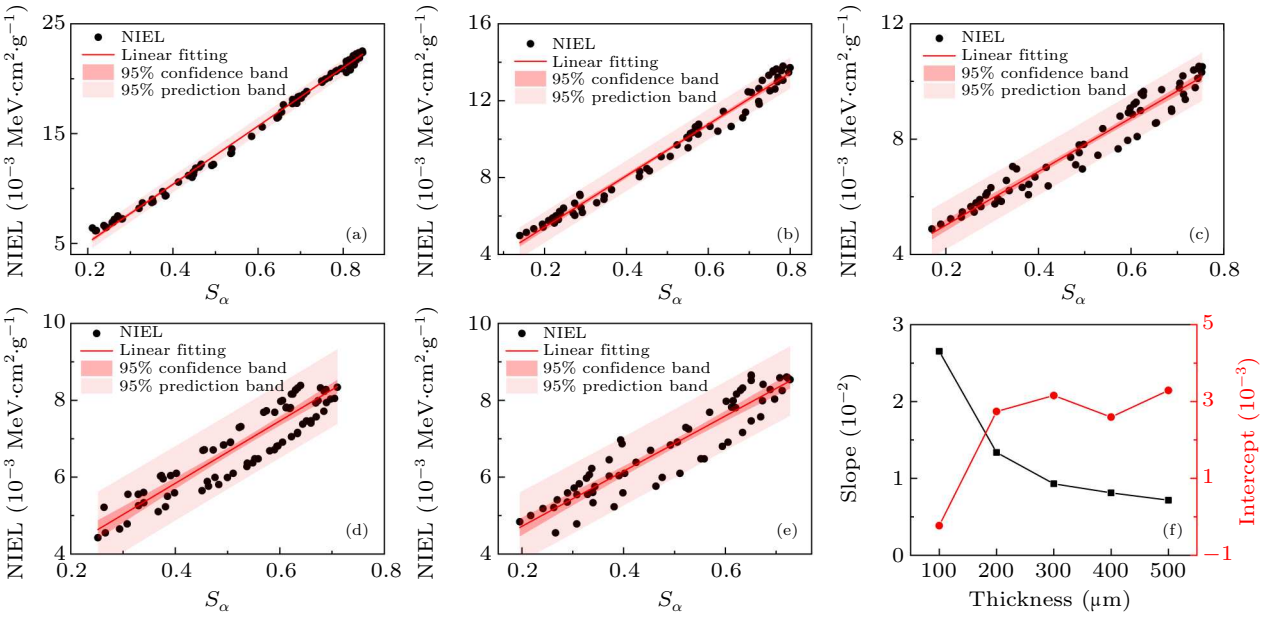


Fig. 6. Correlation between NIEL in GaAs and S_α. Panels (a)–(e) show results for varying GaAs thicknesses: 100 μm, 200 μm, 300 μm, 400 μm, and 500 μm. Panel (f) presents the corresponding fitting parameters.

4.1.1. The distribution of T_{dam}

Shielding layers can significantly alter the spatial distribution of nonionizing energy deposition. Figure 7 shows the distribution of T_{dam} induced by protons under different orbital energy spectra and shielding configurations.

For the case of no shielding, the distribution of T_{dam} in Si decreases with increasing target thickness at each orbital altitude, as shown in Fig. 7(a). This behavior arises from the combined effects of the space broad energy spectrum protons and the energy deposition associated with their Bragg peaks. Specifically, the Bragg peak effect in different energy segments of the broad-spectrum protons causes small T_{dam} when the proton range exceeds the material thickness. When proton ranges lie within the material, their energy is fully deposited, and T_{dam} is mainly limited by the proton flux. Consequently, T_{dam} decreases with increasing material thickness. Additionally, for protons with energies below 1 MeV, the non-ionizing

energy deposition is significantly limited.

With 254 μm Al shielding, the number of protons with energies below 1 MeV decreases substantially, as shown in Fig. 4(c). The evolution of $T_{\rm dam}$ remains similar to the no-shielding case, but its dependence on target thickness is markedly reduced. This is due to the increased proportion of high-energy protons, which shifts the energy deposition characteristics toward higher energies.

For 2.54 mm Al shielding, the proportion of high-energy protons further increases. As a result, the evolution of $T_{\rm dam}$ becomes more uniform and converges to the characteristics of high-energy proton deposition, as shown in Fig. 7(c).

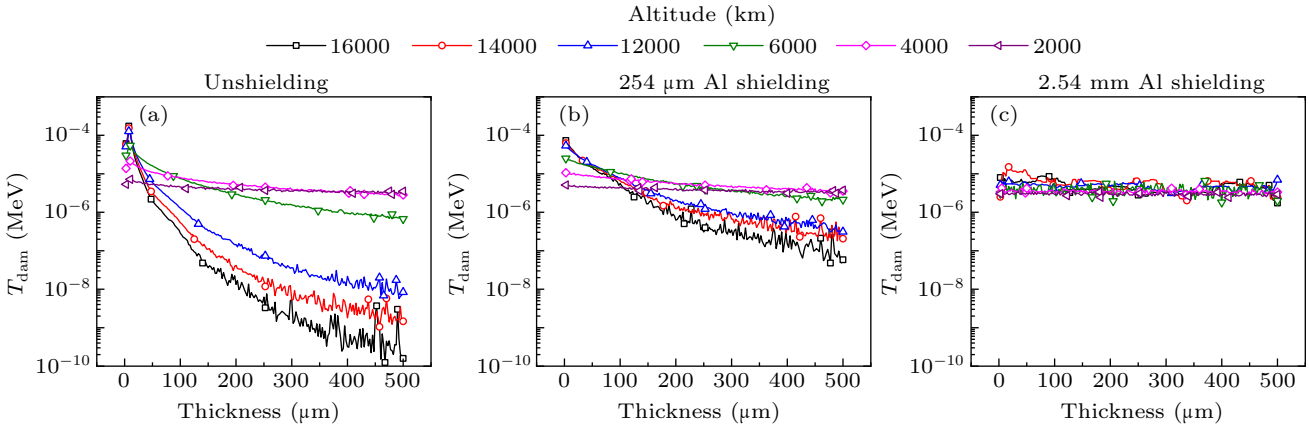


Fig. 7. Distribution of $T_{\rm dam}$ with target thickness for (a) unshielded, (b) 254 μm Al shielding, and (c) 2.54 mm Al shielding. The thickness of the Si material is 500 μm.

4.1.2. The relative contribution of elastic and inelastic NIEL

High-energy proton irradiation induces both elastic and inelastic collisions in materials, with inelastic interactions generating various secondary particles via nuclear reactions or de-excitation processes. These secondary species not only enhance displacement damage, but also increase the total ionizing dose, thereby complicating radiation protection.[36] Consequently, reducing inelastic scattering is crucial for improving radiation shielding performance.

Figure 8 shows the proportion of elastic and inelastic NIEL at different orbital altitudes. The contribution of elastic collisions to NIEL increases with orbital altitude under identical shielding conditions, whereas increasing shielding thickness reduces this contribution at a given altitude.

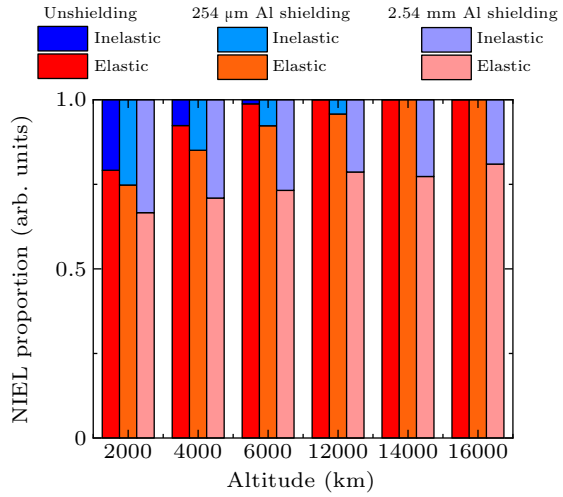


Fig. 8. Proportion of elastic and inelastic NIEL at various orbital altitudes.

For the case of no shielding, the contribution of nuclear inelastic collisions decreases steeply from 20% to below 10% as orbital altitude increases, ultimately falling to less than 0.1% above 12000 km. With 254 μm Al shielding, the contribution of nuclear inelastic collisions significantly increases at each orbital altitude. For 2.54 mm Al shielding, the inelastic collision contribution ranges from 33% at 2000 km to 20% at 16000 km, far exceeding the values observed in unshielded scenarios.

High-energy protons exhibit larger nuclear inelastic scattering cross sections. As the high-energy proton flux decreases with increasing orbital altitude, elastic scattering becomes the dominant interaction mechanism. When a shielding layer is applied, low-energy protons are preferentially absorbed, leading to a higher proportion of nuclear inelastic collisions.

5. Conclusion

In this paper, the displacement damage induced by broad-spectrum protons in semiconductor materials at different orbital altitudes is investigated via Geant4 Monte Carlo simulations. Simulation results show that the NIEL of Si and GaAs initially increases and then decreases with orbital altitude in the absence of shielding. Shielding effects can result in saturation of NIEL or cause it to increase continuously, depending on the shielding thickness.

Effective protons, defined as those with a range of 10% to 120% of the material thickness, are identified. Based on the proportion of effective protons, we propose a fast calculation method for NIEL applicable to arbitrary spectral structures. Increasing shielding thickness and decreasing orbital

altitude modify the incident proton energy spectrum in materials, leading to a more uniform spatial distribution of T_{dam} deposition from broad-spectrum protons. These factors also increase the relative contribution of inelastic collisions to the total NIEL, with 2.54 mm Al shielding raising the inelastic proportion from below 20% to 20%–33%. These findings provide significant insights into the radiation damage effects induced by space protons.

Acknowledgments

Project supported by the National Natural Science Foundation of China (Grant Nos. 12475252, 12175309, and 12175310), the Fund of National University of Defense Technology (Grant No. 22-ZZCX-068), the Strategic Priority Research Program of the Chinese Academy of Sciences (Grant Nos. XDA25050200 and XDA25010100), and the Natural Science Foundation of Hunan Province, China (Grant No. 2025JJ20007).

References

[1] Srour J R, Marshall C J and Marshall P W 2003 *IEEE Trans. Nucl. Sci.* **50** 653
[2] Nordlund K, Zinkle S J, Sand A E, Granberg F, Averback R S, Stoller R E, Suzudo T, Malerba L, Banhart F, Weber W J, Willaime F, Dudarev S L and Simeone D 2018 *J. Nucl. Mater.* **512** 450
[3] Inguimbert C 2025 *Nucl. Instrum. Methods Phys. Res. Sect. B: Beam Interact. Mater. At.* **561** 165622
[4] Srour J R and Palko J W 2013 *IEEE Trans. Nucl. Sci.* **60** 1740
[5] Jay A, Hemeryck A, Richard N, Martin-Samos L, Raine M, Le Roch A, Mousseau N, Goiffon V, Paillet P, Gaillardin M and Magnan P 2018 *IEEE Trans. Nucl. Sci.* **65** 724
[6] Altamura A R, Acerbi F, Di Ruzza B, Verroi E, Merzi S and Gola A 2021 arXiv:2112.08089 [physics.ins-det]
[7] Nordlund K, Zinkle S J, Sand A E, Granberg F, Averback R S, Stoller R, Suzudo T, Malerba L, Banhart F, Weber W J, Willaime F, Dudarev S L and Simeone D 2018 *Nat. Commun.* **9** 1084
[8] Nishiguchi M, Hashinaga T, Nishizawa H, Hayashi H, Okazaki N, Kitagawa M and Fujino T 1990 *IEEE Trans. Nucl. Sci.* **37** 2071
[9] Fleetwood D M 2021 *IEEE Trans. Nucl. Sci.* **68** 509
[10] Kinchin G H and Pease R S 1955 *Rep. Prog. Phys.* **18** 1
[11] Meneghesso G, Paccagnella A, Camin D V, Fedyakin N, Pessina G and Canali C 1997 *IEEE Trans. Nucl. Sci.* **44** 840
[12] Robinson M and Torrens I 1974 *Phys. Rev. B* **9** 5008
[13] Belloir J M, Goiffon V, Virmontois C, Paillet P, Raine M, Magnan P and Gilard O 2016 *IEEE Trans. Nucl. Sci.* **63** 2183
[14] Li J W, Wang Z J, Shi C Y, Xue Y Y, Ning H, Xu R, Jiao Q L and Jia T X 2020 *Acta Phys. Sin.* **69** 098802 (in Chinese)
[15] Jouni A, Sicre M, Malherbe V, Mamdy B, Thery T, Belloir J M, Soussan D, De Paoli S, Lorquet V, Lalucaa V, Virmontois C, Gasiot G and Goiffon V 2023 *IEEE Trans. Nucl. Sci.* **70** 515
[16] Wang Z J, Xue Y Y, Wang Z M, Chen W, Yin L Y, Wang X H, Nie Xu, Lai S K, Huang G, Wang M C, Ding L L, He B P, Ma W Y and Gou S L 2024 *Nucl. Instrum. Methods Phys. Res. Sect. Accel. Spectrometers Detect. Assoc. Equip.* **1058** 168784
[17] Inguimbert C, Arnolda P, Nuns T and Rolland G 2010 *IEEE Trans. Nucl. Sci.* **57** 1915
[18] Chen J, Jung P and Klein H 1998 *J. Nucl. Mater.* **258–263** 1803
[19] Warner J H, Messenger S R, Walters R J, Summers G P, Lorentzen J R, Wilt D M and Smith M A 2006 *IEEE Trans. Nucl. Sci.* **53** 1988
[20] Okuno Y, Okuda S, Akiyoshi M, Oka T, Harumoto M, Omura K, Kawakita S, Imaizumi M, Messenger S R, Lee K H and Yamaguchi M 2017 *J. Appl. Phys.* **122** 114901
[21] Messenger S R, Burke E A, Summers G P, Xapsos M A, Walters R J, Jackson E M and Weaver B D 1999 *IEEE Trans. Nucl. Sci.* **46** 1595
[22] Akkerman A, Barak J, Chadwick M B, Levinson J, Murat M and Lifshitz Y 2001 *Radiat. Phys. Chem.* **62** 301
[23] Jun I, Xapsos M A, Messenger S R, Burke E A, Walters R J, Summers G P and Jordan T 2003 *IEEE Trans. Nucl. Sci.* **50** 1924
[24] Inguimbert C and Gigante R 2006 *IEEE Trans. Nucl. Sci.* **53** 1967
[25] Akkerman A, Barak J and Murat M 2020 *IEEE Trans. Nucl. Sci.* **67** 1813
[26] Akkerman A, Barak J and Murat M 2022 *IEEE Trans. Nucl. Sci.* **69** 2056
[27] Inguimbert C, Durand A, Nuns T and Lemière K 2021 *Nucl. Instrum. Methods Phys. Res. Sect. B Beam Interact. Mater. At.* **490** 7
[28] Messenger S R, Summers G P, Burke E A, Walters R J and Xapsos M A 2001 *Prog. Photovolt. Res. Appl.* **9** 103
[29] Srour J R and Palko J W 2006 *IEEE Trans. Nucl. Sci.* **53** 3610
[30] Hou S H, Dong S L, Yang J Q, Liu Z L, Guan E H, Lin G, Shao G J, Zhang Y B, Jiang J C and Li X J 2025 *IEEE Trans. Nucl. Sci.* **72** 858
[31] Hou S H, Dong S L, Yang J Q, Guan E H, Liu Z L, Shao G J, Zhang Y B and Li X J 2023 *IEEE Trans. Nucl. Sci.* **70** 2590
[32] Inguimbert C 2021 *J. Nucl. Mater.* **559** 153398
[33] Liu L N, Mei B, Zheng Z S, Wang L, Bai Y R, Yu Q K, Li P, Zhao H D, Sun Y C and Li B 2023 *IEEE Trans. Nucl. Sci.* **70** 1885
[34] Parize J, Jarrin T, Fées A, Lambert D, Jay A, Morin V, Hemeryck A and Richard N 2024 *IEEE Trans. Nucl. Sci.* **71** 1461
[35] Ye E L, Lai Y F, Shen C X, Hou Y J and Nan H J 2025 *Radiat. Phys. Chem.* **228** 112417
[36] Jun I 2001 *IEEE Trans. Nucl. Sci.* **48** 162
[37] Xing T, Liu S S, Song C, Wang X, Adekoya M A, Wang C, Li H D, Meng F J, Du X Z, Sun Y F, Zhu S J, Wang L P, Chen W, Li K and Zheng X H 2024 *AIP Adv.* **14** 015142
[38] Bai Y R, Li P, He H, Liu F, Li W and He C H 2024 *Acta Phys. Sin.* **73** 052401 (in Chinese)
[39] Bai Y R, Li Y H, Liu F, Liao L, He H, Yang W T and He C H 2021 *Acta Phys. Sin.* **70** 172401 (in Chinese)
[40] Xue B T, Zhang L M, Liang Y Q, Liu N, Wang D P, Chen L and Wang T S 2023 *Acta Phys. Sin.* **70** 138802 (in Chinese)
[41] Luan N T, Ahn S-W, Hwang Y S, Nam U W, Kang S C and Kim H J 2024 *Nucl. Instrum. Methods Phys. Res. Sect. Accel. Spectrometers Detect. Assoc. Equip.* **1059** 168926
[42] Yang X H, Yu W, Xu H, Zhou H B, Ma Y Y, Zou D B, Yu T P, Ge Z Y, Yin Y and Shao F Q 2014 *Phys. Plasmas.* **21** 063105
[43] Yang X H, Dieckmann M E, Sarri G, Borghesi M 2012 *Phys. Plasmas.* **19** 113110
[44] Yang X H, Ma Y Y, Shao F Q, Xu H, Yu M Y, Gu Y Q, Yu T P, Yin Y, Tian C L and Kawata S 2010 *Laser Part. Beams* **28** 319
[45] Zhong P L, Jiang Y Q, Zi M, Li X C, Zhao N, Deng Y Q, Wu T, Yu R Z, Zhang G B, Yang X H and Ma Y Y 2025 *Acta Phys. Sin.* **74** 065201 (in Chinese)
[46] Wang C Z 2007 *The Research of The Non-ionizing Energy Losses of material by Particles in Space Environment* (Master's Thesis) (Shanghai: Shang Hai University) (in Chinese)
[47] Agostinelli S, Allison J, Amako K, *et al.* 2003 *Nucl. Instrum. Methods Phys. Res. Sect. Accel. Spectrometers Detect. Assoc. Equip.* **506** 250
[48] Allison J, Amako K, Apostolakis J, *et al.* 2006 *IEEE Trans. Nucl. Sci.* **53** 270
[49] Song C, Liu S H, Wang X, Mu H B, Bai Y R, Li H D, Xing T, He C H and Chen W 2023 *Nucl. Instrum. Methods Phys. Res. Sect. B Beam Interact. Mater. At.* **545** 165144
[50] Mendenhall M H and Weller R A 2005 *Nucl. Instrum. Methods Phys. Res. Sect. B Beam Interact. Mater. At.* **227** 420
[51] Li J W, Wang Z J, Shi C Y, Xue Y Y, Ning H, Xu R, Jiao Q L and Jia T X 2020 *Acta Phys. Sin.* **69** 098802 (in Chinese)
[52] Mohamed M, Tariq J, Khalil E H and Ahmed L 2023 *JOM* **75** 3601
[53] Saeide N and Kiazand F 2022 *J. Comput. Electron.* **21** 513
[54] Summers G P, Burke E A, Shapiro P, Messenger S R and Walters R J 1993 *IEEE Trans. Nucl. Sci.* **40** 1372
[55] Gaffey J D and Bilitza D 1994 *J. Spacecr. Rockets* **31** 172
[56] Heynderickx D, Quaghebeur B, Wera J, Daly E J and Evans H D R 2004 *Space Weather* **2** 2004
[57] Ziegler J F, Ziegler M D and Biersack J P 2010 *Nucl. Instrum. Methods Phys. Res. Sect. B Beam Interact. Mater. At.* **268** 1818